Olivine and glass chemistry record cycles of plumbing system recovery after summit collapse events at Kīlauea Volcano, Hawai‘i

Kendra J. Lynn*, Donald A. Swanson

U.S. Geological Survey
Hawaiian Volcano Observatory
1266 Kamehameha Avenue, Suite A-8
Hilo, HI 96720

*corresponding author: klynn@usgs.gov

Keywords: olivine, caldera collapse, Kīlauea, eruptive cycles, Hawai‘i

Published as:
Lynn, K.J. and Swanson, D.A. (2022) Olivine and glass chemistry record cycles of plumbing system recovery after summit collapse events at Kīlauea Volcano, Hawai‘i. *Journal of Volcanology and Geothermal Research*, 426, 107540
doi:10.1016/j.jvolgeores.2022.107540

Abstract

The eruptive activity of Kīlauea Volcano (Hawai‘i) in the past 2,500 years has alternated between centuries-long periods dominated either by explosive or effusive eruptions. The onset of explosive periods appears to be marked by caldera collapse events at the volcano's summit accompanied by draining of Kīlauea's magmatic plumbing system. Here we leverage >1800 olivine forsterite (Fo), >900 glass MgO contents, and estimated magma supply rates from the past six centuries to describe the relationships between summit collapse and the composition of erupted material. On a first order basis, the major element chemistry of the centuries-long eruptive periods largely originates from fundamental differences between fractional crystallization of shallowly stored magmas during high-supply effusive-dominated periods versus little evolution of mafic recharge magmas during low-supply explosive-dominated periods. The modern effusive period (1820s-present) is dominated by relatively evolved olivine forsterite contents (Fo_{81-82}) for Kīlauea, which is interpreted to reflect a buffered crustal reservoir system in which shallow storage and fractional crystallization control the composition of magmas. In contrast, olivine crystals from the explosive Keanakāko‘i Tephra (1500 - early 1800s C.E.) are dominated by higher olivine forsterite contents (Fo_{89}) which are interpreted to reflect more primitive compositions, are correlated with high-MgO glass compositions extending to high values (e.g.,11.0 wt%), and show signs of magma mixing (zoned olivine, bimodal Fo populations). These signatures reflect a disrupted reservoir system in which high-MgO recharge melts mix with melts left over from draining of the shallow (<5 km) magma plumbing.

Superimposed on these explosive-effusive periods are three decades- to centuries long periods of progressively evolving olivine and glass compositions. Eruptions that occur after caldera collapse in ~1500 C.E. and smaller scale crater collapse events in 1790 (inferred) and 1924 have heterogeneous olivine populations dominated by $\geq Fo_{88}$ and typically high MgO glasses. These compositions reflect inefficient mixing of stored and primitive recharge magmas after the disruption of the shallow plumbing system. After these collapses, olivine Fo and glass MgO subsequently evolve to $<Fo_{82}$ and <7.0 wt% compositions, reflecting the recovery of the crustal plumbing system to an end-member system state characterized by efficient mixing of recharge and stored magmas

that serve to buffer the shallow magma reservoirs. These evolved signatures suggest that a mature and buffered reservoir system may be a key condition for significant disruptions of volcanic plumbing systems. Plumbing system recovery is slower following large-scale caldera collapse (hundreds of years) compared to recovery following smaller caldera or crater collapse (tens of years), which may be modulated by differences in magma supply rates. Following the 2018 crater collapse olivine populations have high-Fo but glasses are low MgO, suggesting that this collapse might have disrupted shallow magma pathways but not strongly impacted the reservoir(s). Ultimately, olivine and glass major element chemistry record the impacts of caldera and smaller but significant summit crater collapse events at Kīlauea and could be used to provide a framework for better characterizing long-term volcano evolution in Hawai‘i and shield volcanoes elsewhere.

1. Introduction

Kīlauea is a shield volcano renowned for its frequent eruptions and dominated, since western missionaries arrived in 1823 (Ellis, 1827) by effusive activity, generally within the summit caldera or on rift zones radiating east and southwest from the summit (e.g., Tilling and Dvorak, 1993). Current understanding of Kīlauea's recent eruptive history indicates that centuries-long periods of dominantly explosive eruptive activity occur alternating with intervals of dominantly effusive eruptions, such as those that of the modern period (Swanson et al., 2012, 2014; Swanson and Houghton, 2018). The transition from effusive to explosive periods appears to be punctuated by large-scale caldera collapse (km across in scale), which has occurred at least twice in the past 2,500 years and is thought to be related to the emptying of the summit reservoir system (Powers, 1948; Holcomb, 1987; Swanson et al., 2012; Figure 1). The most recent large-scale caldera collapse and subsequent explosive period began ~1500 C.E., following the 60-yr long ‘Aila‘āu eruption (1410-1470 C.E., Clague et al., 1999; Swanson et al., 2012; Figure 1). Significant but smaller scale summit collapse events (<km in scale) have occurred several times since the formation of the modern summit caldera, the most recent and largest of which was synchronous with the 2018 lower East Rift Zone (LERZ) eruption (Neal et al., 2019).

The impact of summit collapse on the volcano's shallow (<5 km) magmatic plumbing system (regions of magma accumulation, or reservoirs, and pathways between them and the surface) should be recorded in the compositions of erupted melts and their crystal cargo (e.g., Gavrilenko et al., 2016). Lavas recording Kīlauea's past six centuries of eruptive activity are thus ideal for studying the effects of caldera and crater collapse events, in part because Hawaiian tholeiites crystallize only spinel and olivine for >100 °C below the liquidus (Wright and Okamura, 1977; Wright and Peck, 1978; Montierth et al., 1995) and the Fe-Mg contents of olivine and glasses typically reflect the degree of magmatic evolution via crustal processes (e.g., fractional crystallization, magma mixing, shallow storage; Wright and Fiske, 1971; Wright et al., 1975; Wright and Tilling, 1980; Helz, 1987; Helz and Wright, 1992; Wright and Helz, 1996). Additionally, samples of most Kīlauea eruptions show Fe-Mg disequilibrium between olivine cores that are too high in Fo to be in Fe-Mg equilibrium with their host melts (e.g., Maaløe et al., 1988; Garcia et al., 2003; Lynn et al., 2017a, 2017b; Garcia et al., 2018; Wieser et al., 2019) indicating that olivine Fo and glass MgO each record critical but different information about magmatic histories. Thus, using both olivine Fo and glass MgO provides a simple but effective means to broadly describe magmatic histories, allowing one to contrast the character of the magma plumbing system before and after collapse events. Many new studies on the Keanakākoʻi Tephra (ca. 1500 - early 1800s C.E.; Swanson et al., 2012), Kīlauea's most recent explosive period, have also more than doubled our knowledge of the volcano's summit eruptive history (e.g., Swanson et al., 2014; Sides et al., 2014; Lynn et al., 2017b, 2018, 2020; Garcia et al., 2018; Swanson and Houghton, 2018, Biass et al., 2018; Isgett et al., 2018). These factors provide an unprecedented opportunity to leverage geochemical, petrological, and geological datasets to deepen our understanding of Kīlauea's long-term evolution.

Olivine compositions are particularly valuable for such investigations because the forsterite content (Fo, Mg/(Mg+Fe) x 100) is controlled by Fe-Mg equilibrium with the magma in which it grows (e.g., Roeder and Emslie, 1970). Melt MgO content scales with temperature (e.g., Helz and Thornber, 1987) and, by proxy, broadly scales with depth within Kīlauea's reservoir system so that olivine Fo and melt MgO can be used to fingerprint regions of magma storage and evolution prior to eruption (e.g., Helz et al., 2015). Thus, higher Fo olivine are generally inferred to have grown in higher MgO melts deeper within the volcano and at higher temperatures, reflecting olivine control on the magma's major element composition (Figure 2a). Lower Fo olivine reflects growth and/or re-equilibration in shallower, cooler and more fractionated low MgO magmas (Figure 2b). The presence of both high- and low-Fo olivine in an eruption indicate that rising recharge magmas mixed with shallowly stored magmas prior to eruption (Figure 2c). While most Kīlauea eruptions have some range in olivine Fo contents (e.g., Figure 2a), the mode of an eruption's olivine population can be used to discern the dominant magmatic processes that affected the magmatic history (e.g., fractionation versus mixing versus olivine control; Figure 2).

More than 1,800 olivine Fo and 900 glass MgO contents are examined here to characterize the last 500+ years of plumbing-system evolution. We delineate three decades-to-centuries long geochemical cycles within the past ~500 years in which progressively evolving olivine and glass major element compositions are decoupled from inferred changes in mantle-derived magma supply rates to Kīlauea. Eruptions that occur after large-scale caldera collapse have ≥ Fo_{88} olivine populations that can be bimodal (with a low Fo secondary population) and highly heterogeneous glass MgO contents that range up to 11.2 wt%. Subsequent eruptions progressively change toward evolved and typically unimodal olivine Fo (< 82) populations and glass MgO < 7.0 wt% before the next significant crater collapse. This striking difference in composition suggests that large to moderate summit collapses disrupt the shallow reservoir system and influence the dominant magmatic processes controlling the character of erupted material.

2. Methods

2.1. Literature Compilation

Eruptions examined in this study are restricted to summit and upper East Rift Zone locations unless a rift zone eruption was sustained for several years (e.g., Maunaulu 1969-1974, Pu‘u‘ō‘ō 1983-2018). This geographic filter enables the use of olivine and glass chemistry to infer the geometry and processes operating in Kīlauea's summit reservoir(s); otherwise, the olivine and glass chemistry might include the effects of older stored magma in the rift zones that had experienced mixing and fractional crystallization over long periods of time (e.g., 1955 and 1960 LERZ eruptions; Helz and Wright, 1992; Wright and Helz, 1996; Tuohy et al., 2016; and numerous short-lived eruptions in the Nāpau Crater area; Walker et al., 2020). An additional exception is made for the 2018 LERZ eruption, which was the most voluminous known eruption at Kīlauea in more than 500 years, occurred simultaneously with summit crater collapse, and was sustained by summit-derived magma for more than two months (Neal et al., 2019).

Previously published olivine and glass data were examined for analysis quality and oxide totals < 99.0 and > 100.5 were rejected. Studies that reported only representative olivine compositions were not used, and a minimum of 10 olivine compositions in an eruption/sample were required for this dataset (e.g., very few data are available for eruptions between the possible collapse in 1790 and the small collapse and crater enlargement in 1924). We define two broad periods for eruptions included in the study: 1) the Keanakāko‘i Tephra explosive period, which begins with large-scale caldera collapse ~1500 C.E. and ends in the early 1800s (Swanson et al., 2012; Swanson and Houghton, 2018) and 2) the modern effusive period, which begins in this compilation with previously published data for the 1840 eruption (Trusdell, 1991) and ends with December 2020 Halema‘uma‘u eruption samples (this study).

Changes in olivine Fo content over time are assessed by determining compositional modes for individual eruption populations. Kernel density estimates for each eruption are used to identify primary modes based on the highest probability density in the population (Figure 2). A secondary mode is identified (Figure 2c) for some eruption populations that clearly have more than one peak in the distributions, as is also evident in cumulative distribution plots. The kernel density estimates are calculated using a bandwidth of 0.5 mol% because 0.2 mol% (the typical analytical uncertainty in Fo; e.g., following Thomson and Maclennan, 2013) undersmooths and oversamples the data, and normal kernel functions in MATLAB oversmooth and undersample the data (see Supplementary Figure S1 for comparisons). This choice of bandwidth is appropriate because our approach relies on the dominant mode(s) in the populations and not on more subtle variations within eruption datasets. Heterogeneity in individual eruption samples is assessed by calculating the 5^{th} and 95^{th} percentile of the populations, a procedure that minimizes extreme or outlier compositions within the full range of data.

Changes in glass MgO contents with time are examined using the range of available data for each eruption, rather than the population-based approach just described for the olivine compositions. This is done for three reasons: 1) for many summit eruptions, only a few glass MgO contents are reported in the literature (e.g., eruptions from 1868-1954, Helz et al., 2014; Garcia et al., 2003), so that the same statistical treatment cannot be used for all samples; 2) any glass MgO variability within an eruption generally reflects coeval melt compositions sampled from the thermally stratified summit reservoir system (Helz et al., 2014), so that using a mode to represent those data results in loss of information; 3) the MgO content of Kīlauea glasses is a proxy for temperature (Helz and Thornber, 1987), and variations in erupted glass MgO reflect relative residence time, degree of homogenization, and depth of melts sourced from within the reservoir system (Helz et al., 2014).

2.2. Electron Microprobe Analyses (EPMA)

New olivine core compositions (n=133; Lynn, 2022, Supplementary Table S1) from summit (1885, 1921, July 1974, and April 2015 and December 2020) and middle East Rift Zone (ERZ; 2011-2012 Puʻuʻōʻō) eruptions are used in conjunction with previously published olivine from just after caldera collapse around 1500 C.E. to 2018. For new data, measurements were made using a five spectrometer JEOL Hyperprobe JXA-8500F at the University of Hawaiʻi using three different methodologies. Summit eruption analyses (except for those from 2020) did not measure Mn and used *Method 1*: a 20 kV accelerating voltage and a 10 µm beam with a 200 nA current, and peak counting times were 60 s for Si, Fe, Mg, Ca, and Ni. Puʻuʻōʻō analyses included Mn and used *Method 2:* a 20 kV voltage and 10 µm beam with a 200 nA current, and peak counting times were 100 s for Si, Mg, Ca, and Ni, 60 s for Fe, and 30 s for Mn. Backgrounds for all analyses were measured on both sides of the peak for half the peak counting times. The olivine crystals from the recent 2020 eruption were analyzed using *Method 3:* a 15 kV accelerating voltage and a 1 µm beam with a 50 nA current. Major elements Si, Mg, and Fe were gathered using combined EDS analyses on a Thermo UltraDry detector using a SystemSix analyzer with a dead time of 38% and live acquisition for 60 seconds. Ca, Ni, and Mn were measured by WDS spectrometers, and counting times were 60 s with 20 s on both sides of the peak for backgrounds.

For all olivine routines, standards were measured regularly throughout analyses to monitor for instrumental drift. Standards for Methods 1 and 2 were San Carlos olivine (USNM 111312/444; Jarosewich et al., 1980) for Si, Fe and Mg, a synthetic nickel-oxide for Ni, Verma garnet for Mn and Kakanui Augite (USNM 122142; Jarosewich et al., 1980) for Ca. Two-sigma relative precision, based on repeated analyses of San Carlos olivine, are 0.85 wt% for SiO_2, 0.51 wt% for MgO, 0.14 wt% for FeO, 0.019 wt% for NiO, and 0.013 wt% for CaO (Lynn, 2022; Supplementary Table S2). Standards for Method 3 were Springwater olivine (USNM 2566) for Si, Fe, and Mg, a synthetic nickel-oxide for Ni, Verma garnet for Mn and Kakanui Augite (USNM 122142; Jarosewich et al., 1980) for Ca. Two-sigma relative precision, based on repeated analyses of San Carlos olivine, are 0.24 wt% for SiO_2 and MgO, 0.20 wt% for FeO, 0.016 wt% for MnO and NiO, and 0.01 wt% for CaO (Lynn, 2022; Supplementary Table S2).

Major and minor element analyses of glass (Lynn, 2022; Supplementary Table S3) from the same 2020 Halemaʻumaʻu eruption sample analyzed for olivine were made using the University of Hawaiʻi microprobe. Analyses used a 15 kV accelerating voltage and a 10 μm beam with a 10 nA current. Si, Al, and Fe were collected on the same EDS setup listed above with 10% deadtime and live acquisition of 100 s. Peak counting times on WDS spectrometers were 15 s for Mg and Ca, 20 s for Mn, 30 s for Ti, 40 s for Na and K, 70 s for P, and 75 s for S (backgrounds were measured on both sides of the peak for half the peak counting times). Standards for glass analyses were Synthetic Glass (STG-56) for Si, Lake County Plagioclase (USNM 115900; Jarosewich et al., 1980) for Al, Ca, and Na, VG-2 glass (USNM 111240/52; Jarosewich et al., 1980) for Fe and Mg, Ilmenite (USNM 96189; Jarosewich et al., 1980) for Mn and Ti, K-Anorthoclase for K, Fluor-apatite (USNM 104021; Jarosewich et al., 1980) for P, and Troilite for S. Two-sigma relative precision, based on repeated analyses of VG-2 glass, are 0.36 wt% for SiO_2, 0.26 for Al_2O_3, 0.20 for TiO_2, 0.56 wt% for FeO, 0.18 wt% for MnO, 0.08 for MgO, 0.44 wt% for CaO, 0.14 wt% for Na_2O, 0.02 for K_2O, and 0.04 for P_2O_5 and SO_3 (Lynn, 2022; Supplementary Table S4).

For all glass and olivine routines, X-ray intensities were converted to concentrations using standard ZAF corrections (Armstrong, 1988). Analyses with totals <99.0 wt% or >100.5 wt% were rejected. Olivine core compositions from previously published Keanakāko‘i Tephra (n=413; Lynn et al., 2017a, b) and modern effusive eruptions (n=519, 1968-2010; Lynn et al., 2017a) were measured in the same laboratory using generally the same conditions as Methods 1 and 2.

3. Results

Olivine core compositions from the explosive and effusive eruptive periods at Kīlauea are remarkably different. Eruptions during the Keanakāko‘i Tephra explosive period (n=413) have a wide distribution of olivine compositions dominated by high forsterite contents of 88-90 (Figure 3a). Core compositions range from Fo_{77} to Fo_{90} with a minor secondary peak at Fo_{83-84}. Olivine cores from the modern effusive period up to the 2018 LERZ eruption (n=1117) also show a wide range (Fo_{75} to Fo_{90}), but the primary peak of the distribution is Fo_{81} (Figure 3b) with few olivine cores of Fo_{88-89}. The exception during this period is the 1959 Kīlauea Iki eruption, which is dominated by high-Fo compositions (86-90; e.g., Helz, 1987; Vinet and Higgins, 2011) and is well documented to be an eruption that disrupted Kīlauea’s typical summit reservoir system (e.g., Helz, 1987; Richter et al., 1970; Stone and Fleet, 1991; Bradshaw et al., 2018; Helz, 2022).

The olivine distributions for the 2018 LERZ eruption and 2020 summit eruption (n=336) are both strongly bimodal, with the 2018 eruption having a much larger range of compositions down to <Fo_{77} (Figure 3c). These very low Fo compositions are largely due to the location of the 2018 eruption on the LERZ, where a significant volume of evolved stored magma was erupted early in the 2018 eruption sequence (Gansecki et al., 2019). Time period distributions are asymmetrical, indicating that the secondary modes are minor components in erupted materials (except for the 2020 eruption, which is strongly bimodal).

Olivine Fo populations in individual eruptions range widely throughout Kīlauea’s past six centuries. Eruptions that follow large caldera (turn of the 16^{th} century) or smaller-scale crater collapse events in the 18^{th}, 20^{th}, and 21^{st} centuries have highly heterogeneous olivine Fo contents (Fo_{79-90}) and are commonly bimodal (Figure 4; see also Lynn, 2022 and Supplementary Table S5). The primary compositional mode is ≥ Fo_{88} (filled circles), and the low-Fo mode in some samples is usually $Fo_{83\text{-}84}$ (open circles) following caldera collapse ~1500 C.E. (Swanson et al., 2012) and an inferred collapse in 1790 (Swanson et al., 2012; Swanson et al., 2015). After three decades of little eruptive activity following the 1924 Halemaʻumaʻu crater enlargement (Macdonald et al., 1983; Wright and Klein, 2014), the olivine primary mode returned to Fo_{88} in 1959 and Fo_{89} during the Maunaulu eruption in 1969. This pattern is repeated with the most recent 2020 Halemaʻumaʻu eruption in which olivine compositions are bimodal (Fo_{88} and Fo_{82}; Figure 3).

Glass MgO contents after collapse events are also highly heterogeneous within single eruptions, spanning a total range of up to 6.0 wt% in the early 16th, 19th, and mid-20th centuries (Figure 5). Eruptions that follow caldera collapse initiating the Keanakāko'i Tephra period include some of the highest MgO contents (> 11.0 wt%; Figure 5) measured at Kīlauea (Swanson et al., 2014; Garcia et al., 2018). Eruptions in the 1820s (at the end of the Keanakāko'i Tephra period) after the inferred crater collapse in 1790 also have high-MgO glass signatures (up to 10.3 wt%). Following the 1924 Halemʻaumaʻu crater enlargement, the 1934 summit lava has 7.3 wt% MgO glass, and the 1954 lava has low modal olivine (<0.2%) and a bulk rock MgO of 7.0-7.2 wt% (Garcia et al. 2003), suggesting low glass MgO. The first post-1924 high-MgO glass signature is from the 1959 Kīlauea Iki eruption (up to 10.0 wt%), during which magma from a deep source dominated the compositions of erupted material (e.g., Helz, 2022). Notably, the recent 2020 Halemaʻumaʻu eruption had glass MgO near ~7.0 wt% MgO (Figure 5), similar to the eruptions following the 1924 crater enlargement. This suggests that the magnitude of the 2018 observed collapse may not have been large enough to significantly disrupt the magma reservoir(s) and might have only disrupted shallow magma pathways.

In the decades to centuries following collapses, both olivine and glass compositions become less magnesian and are generally accompanied by a reduction in compositional heterogeneity (Figures 3 and 4). During the 17th century, primary olivine compositions decrease slightly from Fo_{89} to Fo_{87}. Glass MgO decreases significantly to as low as 3.8 wt% in juvenile material (Garcia et al., 2018) after violent explosive eruptions and inferred crater collapse in 1790 C.E. From 1950 to 2015, olivine modes decrease from Fo_{89} to Fo_{80} at the summit and to Fo_{79} for the long-lived Puʻuʻōʻō eruption (Figure 4). Glass MgO contents also decrease from a maximum of 10.0 wt% in 1959 to 6.3 wt% in 2015 (Figure 5).

Lava erupted before collapse events has olivine and glass compositions that are significantly evolved compared to those of lava erupted after collapse. Glass MgO contents from ʻAilāʻau flows and Observatory shield flows (Holcomb, 1987; Neal and Lockwood, 2003)) are < 7.0 wt% (Clague et al., 1999; Figure 5). In contrast, most Keanakāko'i Tephra glasses after caldera collapse are on average higher in MgO with higher ranges (up to 11.0 wt% MgO; Figure 5), and their olivine populations are dominated by Fo_{89} compositions (Figure 4). Other eruptions occurring prior to collapses also produce lava with evolved glass chemistry. Juvenile material in Keanakāko'i Unit J1, erupted in 1790 (Swanson and Houghton, 2018) near the end of the explosive period, can be very fractionated (down to 3.6 wt% MgO; Garcia et al., 2018), indicating significant evolution of residual stored magma. In the late 19th and early 20th centuries, nearly aphyric lava flows have < Fo_{82} olivine modes and relatively low-MgO glasses (6.0-6.5 wt%; Figures 4 and 5). The decade-long (2008-2018) summit and 35-year-long Puʻuʻōʻō eruption are also dominated by evolved compositions and precede the 2018 collapse (e.g., Thornber et al., 2015).

Olivine and glass compositions show no systematic variations with inferred or calculated magma supply rates to Kīlauea (Figure 5). The dominantly primitive olivine and high-MgO glasses of the 16th and 17th centuries correlate with low erupted volume and low inferred magma supply rates (5×10^{-4} km^3/yr; Swanson et al., 2014; Figure 5). Similar compositions of primitive olivine Fo and glass MgO occur in early 19th century lava, for which much higher magma supply has been inferred (0.12-0.32 km^3/yr, Wright and Klein, 2014). Further contradiction arises between low-supply, primitive 16th and 17th century eruptions and evolved effusive eruptions during another low-supply period from 1850 to 1924 (Wright and Klein, 2014). Finally, an 8x increase in magma supply from 1950 to 2008 coincides with a dramatic decrease in olivine and glass Mg contents.

4. Discussion

The suite of major element data for olivine and glass from ~1500-2020 C.E. are evaluated below to highlight several observations about the evolution of crustal processes at Kīlauea. Important caveats to acknowledge include that the geologic history of Kīlauea's recent centuries is still being revealed (e.g., Hazlett et al., 2019; Orr et al., 2021; though these new findings are consistent with what was previously inferred), there are few data (and samples) available around the turn of the 20th century and for eruptions prior to the formation of the modern caldera about 500 years ago. However, the available data show on a broad scale that 1) explosive and effusive periods record a spectrum of influences but are dominated by very different magmatic processes and 2) changes in olivine Fo and glass MgO record geochemical cycles on the order of decades to centuries that are linked closely with caldera and significant crater collapses at Kīlauea's summit.

4.1. Explosive and effusive eruptive periods are dominated by fundamentally different magmatic processes

Olivine crystals from the modern effusive period are dominated by relatively evolved Fo_{81} compositions (Figure 3) that reflect a buffered crustal reservoir system in which storage and fractional crystallization control the composition of magmas (e.g., Thornber et al., 2015). The magma storage during high magma supply effusive periods (Wright and Klein, 2014) is generally shallow (<5 km; e.g., Poland et al., 2014), as evidenced by the overall lower glass MgO contents that dominate sustained summit and rift eruptions (Figure 5). In contrast, olivine crystals from the same period are dominated by more primitive $\geq Fo_{88}$ compositions (with a minor secondary population at ~Fo_{83}; Figure 3) and maximum glass MgO contents higher than typically seen during the modern effusive period (e.g., up to 11.3 wt% MgO versus ~10 wt% MgO, respectively; Figure 5). Although evolved compositions are present during the Keanakāko'i explosive period (e.g., glass MgO <6.0 wt%, olivine <Fo_{80}), they do not represent large volumes. Keanakāko'i olivine crystals show clear signs of magma mixing (chemical zoning, bimodal Fo populations; Lynn et al. 2017b) between hotter recharge and residual stored magma bodies shortly prior to eruption during a time when the inferred magma supply rates were much lower (Swanson et al., 2014). Thus, on a first order basis, the major element chemistry of the centuries-long eruptive periods largely originates from fundamental differences between fractional crystallization of shallowly stored magmas during high-supply effusive periods versus little evolution of mafic recharge magmas during low-supply explosive periods.

4.2. Geochemical cycles decades to centuries long track summit collapse

Superimposed on the first order differences between the explosive Keanakāko'i Tephra and modern effusive periods are smaller collapse events that also disrupted the shallow plumbing system (reservoirs, pathways, or both) and the dominant magmatic processes operating within. During pre-collapse eruptions at Kīlauea, lava with evolved olivine and glass compositions repeatedly erupts due to the dominance of fractional crystallization in a mature, stable reservoir system (e.g., Helz et al., 2014a; Thornber et al., 2015). Although magma mixing and/or incorporation of high-Fo mush olivine crystals (e.g., Wieser et al., 2020) does occur (evidenced by a minor population of higher-Fo olivine, Figure 3b), the mafic recharge component is usually buffered by a larger amount of stored magma (Wright and Fiske, 1971; Garcia et al., 2003), and fractional crystallization controls the geochemistry of erupted material.

After caldera collapse, the development of a poorly connected system of dikes or sills (Corbi et al., 2015) results in inefficient mixing of recharge and stored magmas. This evolution has been documented in other volcanic systems, where abrupt changes in the chemistry of erupted material showed a switch from dominantly fractional crystallization to increased magma mixing following collapse events (Gavrilenko et al., 2016). The highly heterogeneous olivine Fo and glass MgO in post-collapse eruptions result from mixing of mafic recharge and minor amounts of stored magmas (e.g., Helz et al., 2015; Lynn et al., 2017b) with more limited influence from fractional crystallization. Thus, timeseries of olivine and glass major element chemistry are strong indicators of the maturity of the magma plumbing system at Kīlauea and elsewhere. Repeated patterns of olivine and glass major element chemistry may also be powerful tools for better forecasts of Kīlauea's eruptive behavior.

4.3. Small collapse events apparently do not impact crustal processes

Small summit collapse events on the order of 100 m of subsidence occurred between 1823 and 1924 when most of Kīlauea's eruptive activity was confined within the summit caldera. At that time, a sustained but diminishing lava lake dominated eruptive activity, with three east rift eruptions (1840, 1922, 1923), and three small caldera and Kīlauea Iki eruptions in 1832, 1868, and 1877 (Orr et al, 2021). Unfortunately, few analyses of glass and olivine exist for these eruptions, only the most recent (e.g., 1885, 1894) lava lake overflows are preserved on the caldera floor, and older flows exposed in 2018 fault scarps remain unsampled. However, highly variable Pb isotopic compositions of lavas from 1912-1924 indicate that the magmas were poorly homogenized, and Pietruszka et al. (2019) inferred that a major disruption to Kīlauea's summit reservoir must have occurred prior to 1912.

The 1885 and 1894 flows are fractionated; glass contains 6.0-7.5 wt% MgO, few olivine phenocrysts (< 2 vol.%), and are clinopyroxene and plagioclase-rich (Garcia et al., 2003). The new olivine analyses for the 1885 lava have a Fo_{79} mode (Figure 4), consistent with a shallow long-lived reservoir buffered to evolved compositions. Major and trace element whole-rock data also indicate efficient mixing of recharge and stored magmas in a single summit reservoir (Pietruszka and Garcia 1999; Garcia et al., 2003) that repeatedly experienced draining and subsidence events on the order of 100 m or more during this time (Macdonald et al., 1983; Wright and Klein, 2014). These small collapse events apparently did not significantly disrupt the shallow reservoir system, although data for this time period are perhaps insufficient to assess the impact of any collapse prior to 1924.

4.4. A geochemical indicator for inferring summit collapse in the geologic record?

Using the patterns in olivine and glass major element chemistry outlined here, time series data might be leveraged to identify unobserved or poorly recorded summit collapse events. The observed enlargement of Halema‘uma‘u crater in 1924 and the possible collapse accompanying the 1790 eruption are thought to have significantly disrupted the summit reservoir system and have been associated with major changes at Kīlauea such as a shift in isotopic composition in 1924 that is probably related to changes in mantle melting productivity (Pietruszka and Garcia, 1999). There is no direct evidence or observations of a large crater collapse in 1790, but mapped fissures and lava flows on the lower East Rift Zone have been interpreted to have formed in 1790 (Moore and Trusdell, 1991; Trusdell and Moore, 2006). This interpretation would be consistent with draining of reestablished summit reservoir(s) and related collapse.

Given these similarities, the additional time series context of olivine and glass major element data further supports a possible collapse in 1790. Beginning with the Keanakāko'i Unit E (~1650 C.E.), primary olivine modes began to decrease (Figure 4) and glass MgO contents continued toward more evolved compositions up to the 1790 eruption (Figure 5). While there are as yet no olivine data for eruptions that occurred between the interbedded circumferential lava flow (1670-1700 C.E.; unit 1790f of Neal and Lockwood, 2003) and Unit K1 (early 1800s) the downward trajectory from 1650-1700 in olivine and glass, and evolved glass composition in 1790, suggest the influence of an increasingly well-established shallow reservoir. These lines of evidence suggest that the decreasing olivine Fo established by 1670 C.E. reflects a geochemical cycle that ended with collapse in 1790. Thus, time series of olivine Fo and glass MgO may be used to identify unobserved or poorly recorded summit collapse events at Kīlauea and elsewhere. These evolved signatures suggest that a mature and buffered reservoir system may be a key requirement for disruptions of volcanic plumbing systems that are significant enough to result in collapse events.

4.5. Reservoir system recovery time influenced by magma supply rates?

On a broad scale, Kīlauea's eruptive cycles apparently correlate with order-of-magnitude changes in inferred magma supply rate to the edifice (Swanson et al., 2014). Inferences of explosive-period magma supply are based on erupted volumes of dominantly tephra deposits around Kīlauea's summit caldera, which may not include any intra-caldera deposits and/or lava flows that might have erupted within the existing deep caldera (possibly greater than 600 m deep; Swanson et al., 2014). Variations in magma supply within explosive periods also cannot be determined with available data. Trace element ratios in Keanakāko'i Tephra glasses also cannot resolve high- versus low-supply debates, as low ratios of highly over moderately incompatible elements (e.g., Nb/Y and La/Yb) might be explained by either higher degrees of partial melting (and thus higher rates of magma supply) or melting of a mantle source that has been previously melted (resulting in lower magma supply to the volcano; Garcia et al., 2018).

Despite these uncertainties for the Keanakāko'i explosive period, magma supply rates that are well constrained for the modern effusive period do not systematically correlate with olivine Fo or glass MgO compositions on the decadal scale (Figures 4 and 5), indicating that the major element composition of olivine and glasses of lava in individual eruptions cannot be predominantly related to changes in magma supply rate. The time series of major element chemistry presented here suggests that magma supply might dictate the rate of magmatic system recovery following disruptive collapse events.

The collapse of Kīlauea's summit caldera in about 1500 C.E. significantly disrupted or destroyed the plumbing system present at the time, possibly leaving behind only small, isolated pockets of stored magma (Swanson et al., 2014; Lynn et al., 2017b; Swanson and Houghton, 2018). Plumbing system recovery was slow during the Keanakāko'i period, with high-Fo olivine modes and high MgO glasses occurring for nearly three centuries until the possible small summit collapse in 1790 C.E. Kīlauea's eruptive output during this time was also ~2% that of the modern effusive period, leading to inferences that magma supply to the volcano following caldera collapse was much lower than during the modern effusive period (Swanson et al., 2014).

Low supply in the absence of a well-established reservoir system during the Keanakāko'i period allows more primitive material to erupt without prolonged crustal storage, yielding heterogeneous olivine populations (Fo_{90-78}; Figure 4) and higher-MgO glasses (6.5-11.1 wt%; Figure 5). Toward the middle of the Keanakāko'i period, bimodal olivine populations with decreasing Fo primary modes and persistent Fo_{83-84} secondary modes (Figure 4) indicate that a shallow, semi-stable reservoir of stored magma was probably being restored (Lynn et al., 2017b). However, the primary modes remain at Fo_{89} for ~200 years after caldera collapse in ~1500 C.E. before starting to evolve, suggesting that plumbing system recovery and reservoir development was slow.

In contrast, the olivine Fo modes evolved rapidly after the 1924 enlargement of Halema'uma'u crater, to Fo_{84} by the end of the Maunaulu eruption 90 years later. Magma supply rates have been calculated to be much higher during the modern effusive period (Figure 5) than during the preceding explosive period, correlating with inferences of a buffered reservoir system (e.g., Thornber et al., 2015), generating low-Fo olivine and low-MgO glasses. Higher supply during the effusive period might explain the faster recovery (e.g., tens of years) of shallow buffering reservoirs compared to the prolonged recovery of the plumbing system in the centuries immediately following caldera collapse.

The roughly two centuries of $\geq Fo_{88}$ modes during the Keanakāko'i period might also reflect more significant disruption of both magma pathways and reservoir(s) compared to the inferred 1790 collapse and 1924 crater enlargement. The recovery cycles following the smaller events in 1790 and 1924 could be much shorter because they disrupted established shallow magma pathways but had little impact on the stability of the shallow reservoir(s). Or the shorter recovery could also be linked to higher supply rates following those events (Wright and Klein, 2014). Thus, it is difficult to confidently link the impact of magma supply to the chemical cycles observed here beyond first order comparisons between explosive and effusive periods.

4.6. Geochemical cycles parallel Holcomb model of Kīlauea's evolution

The olivine and glass major element chemical cycles outlined here roughly parallel cycles of Kīlauea's evolution outlined by Holcomb (1987). Holcomb's caldera-dominated model features shifts in magma storage as successive calderas form, fill, and collapse: "caldera collapse arises from changes in magma plumbing, and collapse in turn causes changes in the plumbing, acting as a feedback mechanism of an oscillatory system… with each perturbation disrupting the plumbing system and followed by evolutionary reintegration of the plumbing system." The evolution from high-Fo olivine and high-MgO glasses to low-Fo olivine and low-MgO glasses three times over the past 500+ years provides evidence of Kīlauea's plumbing system recovery following summit collapse events. Holcomb (1987) also acknowledged that these evolution cycles were "very complicated but possibly predictable harmonic patterns of eruption might ensue," and the chemical cycles outlined here represent additional chemical patterns that track the volcano's evolution via repeating long-term trends.

The progressive change from high-Fo and high-MgO to evolved compositions parallels the proposed eruptive model (Holcomb, 1987), which suggested that rift activity waxed as summit activity waned. Beginning in 1950, a dramatic 8x increase in magma supply over the course of a few decades (Wright and Klein, 2014) led to the development of at least two stable summit magma reservoirs, a larger body at 3-5 km depth and smaller body around 1-2 km depth (Poland et al., 2014; Pietruszka et al., 2015). The decreasing trend of olivine Fo and glass MgO contents in eruptions from 1959 to 2018 (Figures 4 and 5) corroborates interpretations that during periods of high magma supply the magmatic system has increasingly stable shallow reservoirs that buffer magma compositions at lower Mg# (Wright and Fiske, 1971; Garcia et al., 2003).

Sustained rift zone activity is closely linked to the summit reservoir system, requiring a nearly continuous supply of magma to increasingly distant vents (e.g., downrift evolution between Maunaulu, Puʻuʻōʻō, and the 2018 LERZ eruption). Efficient mixing in a 3-5 km deep magma reservoir (e.g., Poland et al., 2014; Pietruszka et al., 2015), in which primitive recharge magmas are buffered by large volumes of resident magma at more evolved compositions, promotes continuously evolving olivine Fo contents and increasingly lower glass MgO contents. This interpretation explains why more primitive Fo contents (> Fo_{85}) have only rarely been observed in the past 30 years (with the exception of the 2018 LERZ eruption [Wieser et al., 2020; Lerner et al., 2021] and the recent 2020-2021 Halemaʻumaʻu eruption).

Although the geochemical cycles presented here generally agree with the Holcomb (1987) model, that model was developed during a time where there were few radiometric ages and little knowledge of the explosive history of Kīlauea. The collapses in the Holcomb model are mostly small compared to caldera forming events that mark a change from an effusive to an explosive period (Swanson et al., 2014). Those much larger collapses impact the magmatic system profoundly, as evidenced by the centuries of reservoir recovery recorded by glass and olivine following the caldera formation in 1500 C.E. The ensuing centuries of eruptive activity may be associated with much smaller events (e.g., 1790, 1924, 2018), constituting elements of the Holcomb model. Furthermore, evidence of an effusive eruption low on the East Rift Zone has not been recognized before the 1500 C.E. summit collapse, so the close relation between summit collapse and LERZ eruptions implied by the Holcomb model (Holcomb et al., 1988) remains problematic. Further geochemical study of the transition from the Observatory Shield and subsequent ʻAilāʻau flows (Holcomb, 1987; Neal and Lockwood, 2003; 1000-

1500 C.E.) to the Keanakāko'i Tephra period will yield critical insights into the processes that lead to large caldera forming events. However, the major element geochemical cycles described here help to distinguish between the larger effusive-explosive cycle identified by Swanson et al. (2014) and the smaller Holcomb (1987) cycles.

4.7. The 2018 summit collapse may have had minimal impact on reservoirs

The recent 2018 LERZ eruption and coeval summit collapse (Neal et al., 2019) is an important demonstration of how such events can affect the major element chemistry of subsequent eruptions. A large intrusion into the LERZ that began in May 2018 partially drained the shallow Halema'uma'u reservoir (Anderson et al. 2019), leading to the most significant collapse event in the past 200 years (Neal et al., 2019). After a little over 2 years of subsequent quiescence, eruptive activity returned to Kīlauea's summit in Halema'uma'u crater in December 2020. The return of eruptive activity in the summit fits with the Holcomb (1987) model, wherein summit collapse might interrupt dikes transporting magma into rift zones (Fiske and Jackson, 1972) and subsequently cause changes in long-term eruption patterns.

Prior to the 2018 summit collapse, lava flows from Pu'u'ō'ō had glass MgO contents around 6.3 wt% (Figure 5), similar to the flows in the Observatory Shield and 'Ailā'au flow field (Clague et al., 1999) that predate the modern caldera. The recurrence of evolved compositions prior to significant summit collapse events indicates that the development of a semi-stable and volumetrically significant reservoir might be necessary before collapse can occur. The presence of this reservoir is evidenced by the evolved olivine and melt compositions, which are useful indicators of a mature plumbing system that can be applied to the older eruptive record.

Following the 2018 collapse, the 2020 summit eruption yielded a bimodal population of olivine compositions with a peak at Fo_{88}, following the patterns defined by the previous ~500 years of activity (Figure 4). Notably, the composition of glass in the 2020 tephra did not rebound and instead clusters around ~7.0 wt% MgO, consistent with fractionated magmas (Figure 5). These low-MgO glasses are very different from the high MgO glass compositions that followed caldera collapse in 1500 C.E., yet similar to the few geochemical data for eruptions shortly after the 1924 crater enlargement (7.0-8.0

wt% MgO; Figure 5). Thus, the impacts of the 2018 collapse appear to be on a much smaller scale, and potentially caused by different processes, than those resulting from caldera formation in 1500 C.E. Despite the dramatic events of 2018 the collapse may have only disrupted magma pathways and not strongly impacted the reservoir(s), consistent with models showing that only 11-33% of the total magma in the shallow Halemaʻumaʻu reservoir was withdrawn by the 2018 eruption (Anderson et al., 2019). Alternatively, high magma supply evidenced by two order of magnitude increases in seismicity underneath the Island of Hawaiʻi (beginning in 2015 and ongoing; Burgess and Roman, 2021) may be driving accelerated system recovery after the collapse.

5. Conclusions

Major element chemistry in olivine and glass from Kīlauea's past 500+ years provides simple yet powerful tools for interpreting changes in the crustal reservoir system and the dominant magmatic processes operating within it. The most recent explosive and effusive periods are dominated by fundamentally different crustal processes. The Keanakāko'i Tephra explosive period is characterized by recharge of mafic magmas with little storage in a disrupted reservoir system during a period of overall lower magma supply. During the modern effusive period mafic recharge magmas are buffered by magma reservoirs that are capable of sustaining long-lived eruptions during periods of higher magma supply. Both periods show that magma mixing is a ubiquitous process at Kīlauea, regardless of explosive versus effusive period distinction.

Superimposed on the explosive-effusive periods are three decades- to centuries-long cycles of increasingly evolved olivine Fo and glass MgO in 500+ years of Kīlauea lavas and tephra. Each cycle apparently begins with a caldera or crater collapse event, inferred to disrupt the magmatic system. Prior to caldera and crater collapse, olivine and glass compositions are fractionated, suggesting that a mature and buffered reservoir system may be a key requirement for disruptions of volcanic plumbing systems that are significant enough to result in collapse events. Eruptions that follow collapse events typically reflect mafic compositions, suggesting inefficient mixing of recharge and stored magmas in the absence of a volumetrically significant stable reservoir. The historically unprecedented 2018 summit collapse generally follows these patterns, with evolved olivine and glass compositions at the summit and Puʻuʻōʻō prior to collapse and Fo_{88} olivine in the subsequent 2020 eruption. Thus, significant summit collapse events appear to fundamentally change at least the connectivity of the crustal reservoir system, the dominant magmatic processes operating within it, and ultimately the major element compositions of subsequently erupted material at Kīlauea. The geochemical cycles outlined here are useful for inferring past collapse events that were not observed, and the concepts could be applied broadly to investigate caldera collapse and the long-term evolution of volcanic systems in Hawaiʻi and elsewhere.

6. Acknowledgements

Early work was supported by National Science Foundation grants OISE-1513668 and EAR-1939964 to K.J. Lynn. This work would not have been possible without Stephen T. Allard and the support of the Volcano Science Center Writing Group. We thank Joseph R. Boro for assistance with microprobe analyses of 2020 eruption tephra, Michael O. Garcia for supplying summit and Puʻuʻōʻō samples for the new analyses in this study, Elisabeth Gallant for discussions about population statistics and kernel density estimates, and Michael O. Garcia, Thomas Shea, Timothy Rose, and Thomas L. Wright for productive discussions during the development of these ideas. An early version of this manuscript benefitted greatly from a detailed review by Thomas L. Wright. We thank Jim Gardner for editorial handling and Silvio Mollo, R. Lopaka Lee, and an anonymous reviewer for comments that improved this manuscript. Any use of trade, firm, or product names is for descriptive purposes only and does not imply endorsement by the U.S. Government.

7. References

Anderson, K.R., Johanson, I.A., Patrick, M.R., Gu, M., Segall, P., Poland, M.P., Montgomery-Brown, E.K., Miklius, A., 2019. Magma reservoir failure and the onset of caldera collapse at Kīlauea Volcano in 2018, Science, 366, eaaz1822. doi: 10.1126/science.aaz1822

Armstrong, T.T., 1988. Quantitative analyses of silicate and oxide materials: Comparison of Monte Carlo, ZAF, and φ(ρz) procedures. In: *Microbeam Analyses*, San Francisco Press, San Francisco, 239-246.

Biass, S., Swanson, D.A., Houghton, B.F., 2018. New perspective on the nineteenth-century golden pumice deposit of Kīlauea Volcano. In: Poland, M.P., Garica, M.O., Camp, V.E., and Grunder, A. (Eds.), Field Volcanology: A tribute to the distinguished career of Don Swanson. Geol. S. Am. S.., 538, 191-202. doi: 10.1130/2018.2538(10)

Bradshaw, R.W., Kent, A.J.R., Tepley, F.J., 2018. Chemical fingerprints and residence times of olivine in the 1959 Kilauea Iki eruption, Hawai‘i: Insights into picrite formation. Am. Mineral. 103, 1812-1826. doi: 10.2138/am-2018-6331

Burgess, M.K., Roman, D.C., 2021. Ongoing (2015-) magma surge in the upper mantle beneath the island of Hawai‘i. Geophs. Res. Lett. 48, e2020GL091096. doi: 10.1029/2020GL091096

Clague, D.A., Hagstrum, J.T., Champion, D.E., Beeson, M.H., 1999. Kīlauea summit overflows: Their ages and distribution in the Puna District, Hawai‘i. B. Volcanol. 61, 363-381. doi: 10.1007/s004450050279

Corbi, F., Rivalta, E., Pinel, V., Maccaferri, F., Bagnardi, M., Acocella, V., 2015. How caldera collapse shapes the shallow emplacement and transfer of magma in active volcanoes. Earth Planet Sc. Lett. 431, 287-293, doi: 10.1016/j.epsl.2015.09.028.

Ellis, W., 1827. Narrative of a tour through Hawaii, or Owhyhee; With observations on the natural history of the Sandwich Islands, and remarks on the manners, customs, traditions, history, and language of their inhabitants. H Fisher, Son, and P. Jackson, 2nd ed., 480 p.

Fiske, R.S., Jackson, E.D., 1972. Orientation and growth of Hawaiian volcanic rifts: The effect of regional structure and gravitational stresses. Proc. R. Soc. Lond. A, 329, 299-326. doi: 10.1098/rspa.1972.0115

Gansecki, C., Lee, R. L., Shea, T., Lundblad, S. P., Hon, K.,Parcheta, C., 2019. The tangled tale of Kīlauea's 2018 eruption as told by geochemical monitoring. Science, 366(December), 1–9. doi: 10.1126/science.aaz0147

Garcia, M.O., Pietruszka, A.J., Rhodes, J.M., 2003. A petrologic perspective of Kīlauea Volcano's summit magma reservoir. J. Petrol. 44, 2313-2339. doi: 10.1093/petrology/egg079

Garcia, M.O., Mucek, A.E., Lynn, K.J., Swanson, D.A., Norman, M.D., 2018. Geochemical evolution of Keanakāko'i Tephra, Kīlauea Volcano, Hawai'i. In: Poland, M.P., Garica, M.O., Camp, V.E., and Grunder, A. (Eds.), Field Volcanology: A tribute to the distinguished career of Don Swanson. Geol. S.Am. S., 538, 203-225. doi: 10.1130/2018.2538(09)

Gavrilenko, M., Ozerov, A., Kyle, P.R., Carr, M.J., Nikulin, A., Vidito, C., Danyushevsky, L., 2016. Abrupt transition from fractional crystallization to magma mixing at Gorely volcano (Kamchatka) after caldera collapse. B. Volcanol. 78, 1-47. doi: 10.1007/s00445-016-1038-z

Hazlett, R.W., Orr, T.R., Lundblad, S.P., 2019. Undocumented late 18th- to early 19th-century volcanic eruptions in the southwest rift zone of Kīlauea Volcano, Hawai'i. USGS Sci. Inv. Rep., 5010, 13 p. doi: 10.3133/sir20195010

Helz, R.T., 1987. Diverse olivine types in lava of the 1959 eruption of Kilauea Volcano and their bearing on eruption dynamics, in Decker, R.W., Wright, T.L., Stauffer, P.H., (Eds.), Volcanism in Hawaii. USGS Prof. Pap. 1350, 691-722.

Helz, R.T., 2022. Proportions, timing, and re-equilibration progress during the 1959 summit eruption of Kīlauea: An example of magma mixing processes operating during OIB petrogenesis, J. Petrol, egab091. doi: 10.1093/petrology/egab091.

Helz, R.T., Thornber, C.R., 1987. Geothermometry of Kilauea Iki lava lake, Hawaii. Bull. Volcanol., 49, 651-668. doi: 10.1007/BF01080357

Helz, R.T., Banks, N.G., Heliker, C., Neal, C.A., Wolfe, E.W., 1995. Comparative geothermometry of recent Hawaiian eruptions. J. Geophys. Res. 100, 17,637-17,657. doi: 10.1029/95JB01309

Helz, R.T., Clague, D.A., Sisson, T.W., and Thornber, C.R., 2014a. Petrologic insights into basaltic volcanism at active Hawaiian volcanoes, in Poland, M.P., Garcia, M.O., Camp, V.E., Grunder, A., (Eds.), Characteristics of Hawaiian Volcanoes. USGS Prof. Pap. 1801, 237-292. doi: 10.3133/pp18016

Helz, R.T., Clague, D.A., Mastin, L.G., and Rose, T.R., 2014b. Electron microprobe analyses of glasses from Kīlauea tephra units, Kīlauea Volcano, Hawai‘i. USGS Open File Rep. 2014-1090, 24 p. doi: 10.3133/ofr20141090

Helz, R.T., Clague, D.A., Mastin, L.G., Rose, T.R., 2015. Evidence for large compositional ranges in coeval melts erupted from Kīlauea’s summit reservoir, in Carey, R., Cayol, V., Poland, M., Weis, D., (Eds.), Hawaiian Volcanoes: From Source to Surface. AGU Geophys. Mono. 208. 125-145. doi: 10.1002/9781118872079

Helz, R.T., Wright, T.L., 1992. Differentiation and magma mixing on Kilauea’s east rift zone: A further look at the eruptions of 1955 and 1960. Part 1. The late 1955 lavas. B. Volcanol., 54, 361-384. doi: 10.1007/BF00312319

Holcomb, R.T., 1987, Eruptive history and long-term behavior of Kilauea Volcano, in Decker, R.W., Wright, T.L., Stauffer, P.H., (Eds.), Volcanism in Hawaii. USGS Prof. Pap. 1350. 261-350.

Holcomb, R.T., Moore, J.G., Lipman, P.W., Belderson, R.H., 1988, Voluminous submarine lava flows from Hawaiian volcanoes. Geology, 16, 400-404. doi: 10.1130/ 0091-7613(1988)016<0400:VSLFFH>2.3.CO;2

Isgett, S.J., Houghton, B.F., Swanson, D.A., 2018. Eruption and emplacement dynamics of coarse-grained, wall-rock rich beds in the Keanakāko’i Tephra, Kīlauea, Hawai‘i. In: Poland, M.P., Garica, M.O., Camp, V.E., and Grunder, A., (Eds.), Field Volcanology: A tribute to the distinguished career of Don Swanson. Geol. S. A. S., 538, 191-202. doi: 10.1130/2018.2538(08)

Jarosewich, E., Nelen, J.A., Norberg, J.A., 1980. Reference samples for electron microprobe analysis. Geos. News. 4, 43-47. doi: 10.1111/j.1751-908X.1980.tb00273.x

Lerner, A. H., Wallace, P. J., Shea, T., Mourey, A. J., Kelly, P. J., Nadeau, P. A., Elias, T., Kern, C., Clor, L. E., Gansecki, C., Lee, R. L., Moore, L. R., Werner, C. A. (2021). The petrologic and degassing behavior of sulfur and other magmatic volatiles from the 2018 eruption of Kīlauea, Hawai‘i: melt concentrations, magma storage depths, and magma recycling. B. Volcanol., 83(6), 43. doi: 10.1007/s00445-021-01459-y

Lynn, K.J., 2022. Olivine and glass analyses for select eruptions of Kīlauea Volcano, Hawai‘i. USGS Data Release, doi: 10.5066/P9HA3PRK

Lynn, K. J., Shea, T., Garcia, M. O., 2017a. Nickel variability in Hawaiian olivine: Evaluating the relative contributions from mantle and crustal processes. Am. Min., 102, 507–518. doi: 10.2138/am-2017-5763

Lynn, K. J., Garcia, M. O., Shea, T., Costa, F., Swanson, D. A., 2017b. Timescales of mixing and storage for Keanakāko‘i Tephra magmas (1500–1820 C.E.), Kīlauea Volcano, Hawai‘i. Con. Min. Pet., 172(9). doi: 10.1007/s00410-017-1395-4

Lynn, K.J., Shea, T., Garcia, M.O., Costa, F., Norman, M.D., 2018. Lithium diffusion in olivine records magmatic priming of explosive basaltic eruptions. Earth Planet. Sci. Lett., 500, 127-135. doi: 10.1016/j.epsl.2018.08.002

Lynn, K.J., Garcia, M.O., Shea, T., 2020. Phosphorus coupling obfuscates lithium geospeedometry in olivine. Front. Earth Sci., 8, 135. doi: 10.3389/feart.2020.00135

Maaløe, S., Pederson, R.B., James, D., 1988. Delayed fractionation of basaltic lavas. Cont. Min. Pet., 98, 401-407.

Macdonald, G.A., Abbott, A.T., Peterson, F.L., 1983. Volcanoes in the Sea: The Geology of Hawaii. Univ.Hawaii Press, Honolulu, HI, 517 p.

Montierth, C., Johnston, A.D., Cashman, K.V., 1995. An empirical glass-composition-based geothermometer for Mauna Loa lavas, in Rhodes J.M., Lockwood, J.P., (Eds.), Mauna Loa Revealed: Structure, Composition, History, and Hazards. AGU Geophys. Mono. 92, 201-217. doi: 10.1029/GM092p0207

Moore, R.B., Trusdell, F.A., 1991. Geologic map of the lower east rift zone of Kilauea Volcano, Hawaii. USGS IMAP, 2225. doi: 10.3133/i2225

Neal, C.A., et al., 2019. The 2018 rift eruption and summit collapse of Kīlauea Volcano. Science, 363, 367-374. doi: 10.1126/science.aav7046

Neal, C.A., Lockwood, J.P., 2003. Geologic map of the summit region of Kīlauea Volcano, Hawaii. USGS Geol. Inves. Ser. I, 2759. doi: 10.3133/i2759

Orr, T.R., Hazlett, R., DeSmither, L., Kauahikaua, J., Gaddis, B., 2021. Correcting the historical record for Kīlauea Volcano’s 1832, 1868, and 1877 summit eruptions. J. Volcanol. Geotherm. Res., 410, 107168. doi: j.jvolgeores.2020.107168

Pietruszka, A.J., Garcia, M.O., 1999. A rapid fluctuation in the mantle source and melting history of Kilauea volcano inferred from geochemistry of its historical summit lavas (1790-1982). J. Petrol. 40, 1321-1342. doi: 10.1093/petroj/40.8.1321

Pietruszka, A.J., Heaton, D.E., Garcia, M.O., Marske, J.P., 2019. Explosive summit collapse of Kīlauea Volcano in 1924 preceded by a decade of crustal contamination and anomalous Pb isotope ratios. Geochim. Cosmochim. Acta, 258, 120-137. doi: 10.1016/j.gca.2019.05.029

Pietruszka, A.J., Heaton, D.E., Marske, J.P., Garcia, M.O., 2015. Two magma bodies beneath the summit of Kilauea volcano unveiled by isotopically distinct melt deliveries from the mantle. Earth Planet. Sci. Lett. 413, 90-100. doi: 10.1016/j.epsl.2014.12.040

Poland, M.P., Miklius, A., Sutton, A.J., Thornber, C.R., 2012. A mantle-driven surge in magma supply to Kīlauea Volcano during 2003-2007. Nature Geos., 5, 295-300. doi: 10.1038/ngeo1426

Poland, M.P., Miklius, A., Montgomery-Brown, E.K., 2014. Magma supply, storage, and transport at shield-stage Hawaiian volcanoes, in Poland, M.P., Garcia, M.O., Camp, V.E., Grunder, A., (Eds.), Characteristics of Hawaiian Volcanoes. USGS Prof. Pap. 1801, 179-234. doi: 10.3133/pp10815

Powers, H.A., 1948. A chronology of the explosive eruptions at Kilauea. Pacific Sci. 2, 278-292.

Roeder, P.L., Emslie, R.F., 1970. Olivine-liquid equilibrium, Cont. Mineral. Petrol., 29, 275-289. doi: 10.1007/BF00371276

Richter, D.H., Eaton, J.P., Murata, K.J., Ault, W.U., Krivoy, H.L., 1970. Chronological narrative of the 1959-1960 eruption of Kilauea Volcano, Hawai‘i. USGS Prof. Pap. 537-E, 1-70.

Sides, I.R., Edmonds, M., Maclennan, J., Swanson, D.A., Houghton, B.F., 2014. Eruption style at Kīlauea Volcano in Hawai‘i linked to primary melt composition. Nature Geos., 7, 464-469. doi: 10.1038/ngeo2140

Stone, W.E., Fleet, M.E., 1991. Nickel-copper sulfides from the 1959 eruption of Kilauea volcano, Hawai‘i: Contrasting compositions and phase relations in eruption pumice and Kilauea Iki lava lake. Am. Mineral., 76, 1363-1372.

Swanson, D.A., Rose, T.R., Fiske, R.S., McGeehin, J.P., 2012. Keanakākoʻi Tephra produced by 300 years of explosive eruptions following collapse of Kīlauea's caldera in about 1500 CE. J. Volc. Geotherm. Res. 215-216, 8-25, doi: 10.1016/j.jvolgeores.2011.11.009.

Swanson, D.A., Rose, T.R., Mucek, A.E., Garcia, M.O., Fiske, R.S., Mastin, L.G., 2014, Cycles of explosive and effusive eruptions at Kilauea Volcano, Hawaii. Geology 42, 631-634. doi: 10.1130/G35701.1

Swanson, D.A., Weaver, S.J., Houghton, B.F., 2015. Reconstructing the deadly eruptive events of 1790 CE at Kīlauea Volcano, Hawaiʻi. Geol. S. Am. Bull., 127, 503-515. doi: 10.1130/B31116.1

Swanson, D.A., and Houghton, B.F., 2018. Products, processes, and implications of Keanakāko'i volcanism, Kīlauea Volcano, Hawaiʻi. In: Poland, M.P., Garica, M.O., Camp, V.E., and Grunder, A. (Eds.), Field Volcanology: A tribute to the distinguished career of Don Swanson. Geol. S. Am. S., 538, 159-202. doi: 10.1130/2018.2538(07)

Thomson, A., Maclennan, J., 2013. The distribution of olivine compositions in Icelandic basalts and picrites. J Petrol. 54, 745-768. doi: 10.1093/petrology/egs083

Thornber, C.R., Orr, T.R., Heliker, C., Hoblitt, R.P., 2015. Petrologic testament to changes in shallow magma storage and transport during 30+ years of recharge and eruption at Kīlauea Volcano, Hawaiʻi, in Carey, R., Cayol, V., Poland, M.P., Weis, D., (Eds.), Hawaiian Volcanoes: From Source to Surface. AGU Geophys. Monog. 208, 147-188. doi: 10.1002/9781118872079.ch8

Tilling, R.I., Dvorak, J.J., 1993. Anatomy of a basaltic volcano, Nature, 363, 125-133. doi: 10.1038/363125a0

Trusdell, F.A., 1991. The 1840 eruption of Kilauea Volcano: Petrologic and volcanologic constraints on rift zone processes. [M.S. thesis]: Honolulu, Univ. Hawaiʻi, 109 p.

Trusdell, F.A., Moore, R.B., 2006. Geologic map of the middle east rift geothermal subzone, Kīlauea Volcano, Hawaiʻi. USGS IMAP, 2614. doi: 10.3133/i2614

Tuohy, R.M., Wallace, P.J., Loewen, M.W., Swanson, D.A., Kent, A.J.R., 2016. Magma transport and olivine crystallization depths in Kīlauea's east rift zone inferred from experimentally rehomogenized melt inclusions. Geochim. Cosmochim. Acta, 185, 232-250. doi: 10.1016/j.gca.2016.04.020

Vinet, N., Higgins, M.D., 2010. Magma solidification processes beneath Kilauea Volcano, Hawaii: A quantitative texture and geochemical study of the 1969-1974 Mauna Ulu lavas. J. Petrol. 51, 1297-1332. doi: 10.1093/petrology/egq020

Vinet, N., Higgins, M.D., 2011. What can crystal size distributions and olivine compositions tell us about magma solidification processes inside Kilauea Iki lava lake, Hawaii? J. Volcanol. Geotherm. Res. 208, 136-162. doi: 10.1016/j.volgeores.2011.09.006

Walker, B.H., Garcia, M.O., Orr, T.R., 2020. Petrologic insights into rift zone magmatic interactions from the 2011 eruption of Kīlauea Volcano, Hawai‘i. J. Petrol., 60, 2051-2076. doi: 10.1093/petrology/egz064

Wieser, P. E., Lamadrid, H., Maclennan, J., Edmonds, M., Matthews, S., Iacovino, K., Jenner, F. E., Gansecki, C., Trusdell, F., Lee, R. L., Ilyinskaya, E., 2021. Reconstructing Magma Storage Depths for the 2018 Kīlauean Eruption from Melt Inclusion CO2 Contents: The Importance of Vapor Bubbles. Geochem. Geophys. Geosys., 22, 1–30. doi: 10.1029/2020GC009364

Wieser, P. E., Edmonds, M., Maclennan, J., Wheeler, J., 2020. Microstructural constraints on magmatic mushes under Kīlauea Volcano, Hawai‘i. Nat. Comm., 11:14. doi: 10.1038/s41467-019-13635-y

Wieser, P.E., Edmonds, M., Maclennan, J., Jenner, F.E., Kunz, B.E., 2019. Crystal scavenging from mush piles recorded by melt inclusions. Nat. Comm. 10, 5797. doi: 10.1038/s41467-019-13518-2

Wright, T.L., Fiske, R.S., 1971. Origin of the differentiated and hybrid lavas of Kilauea Volcano, Hawaii. J. Petrol. 12, 1-65. doi: 10.1093/petrology/12.1.1

Wright, T.L., Swanson, D.A., Duffield, W.A., 1975. Chemical compositions of Kilauea east-rift lava, 1968-1971. J. Petrol., 16, 110-133. doi: 10.1093/petrology/16.1.110

Wright, T.L., Okamura, R.T., 1977. Cooling and crystallization of tholeiitic basalt, 1965 Makaopuhi Lava Lake, Hawaii. USGS Prof. Pap., 1004, 1-78. doi: 10.3133/pp1004

Wright, T.L., Peck, D.L., 1978. Crystallization and differentiation of the Alae magma, Alae lava lake, Hawaii. USGS Prof. Pap. 935, 1-19. doi: 10.3133/pp935C

Wright, T.L., Helz, R.T., 1996. Differentiation and magma mixing on Kīlauea's east rift zone: A further look at the eruptions of 1955 and 1960. Part II. The 1960 lavas. Bull. Volcanol. 57, 602-630.

Wright, T.L., Tilling, B.I., 1980. Chemical variations in Kilauea eruptions 1971-1974. Am. J. Sci., 280-A, 777-793.

Wright, T.L., Helz, R.T., 1996. Differentiation and magma mixing on Kilauea's east rift zone: a further look at the eruptions of 1955 and 1960 Part II. The 1960 lavas. B. Volcanol. 57, 602-630. doi: 10.1007/s004450050115

Wright, T.L., Klein, F.W., 2014. Two hundred years of magma transport and storage at Kīlauea Volcano, Hawaii, 1790-2008. USGS Prof. Pap. 1806, 1-240. doi: 10.3133/pp1806

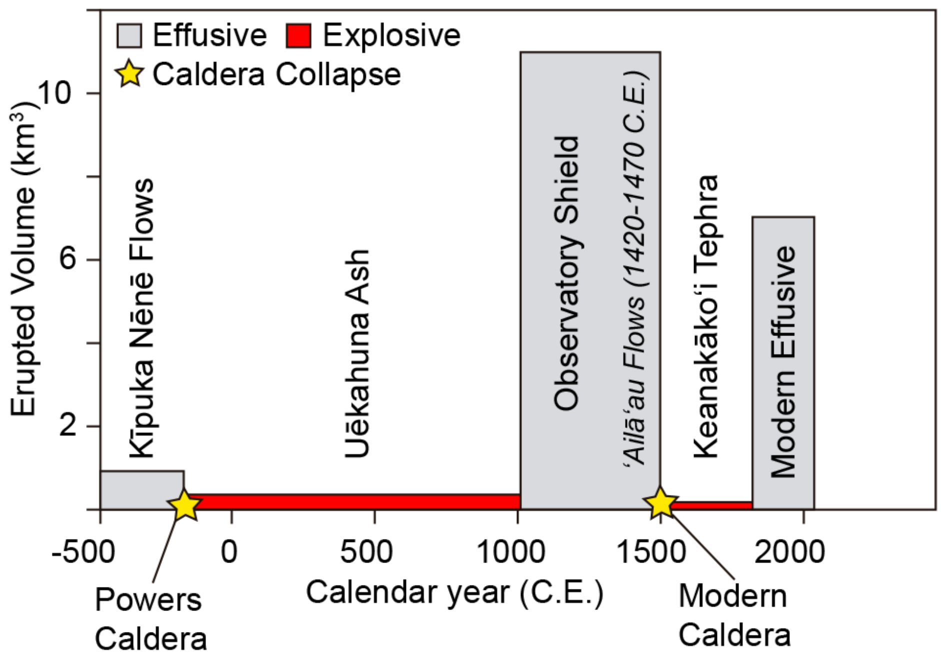

Figure 1: Erupted volume (km^3) for effusive (grey bins) and explosive periods (red bins) in the past 2,500 years at Kīlauea. Yellow stars indicate large caldera collapse events (Powers, 1948; Holcomb, 1987; Swanson et al., 2012). Modified after Swanson et al. (2014). Note that Uēkahuna = Uwēkahuna; name updated in 2012, U.S. Board on Geographic Names.

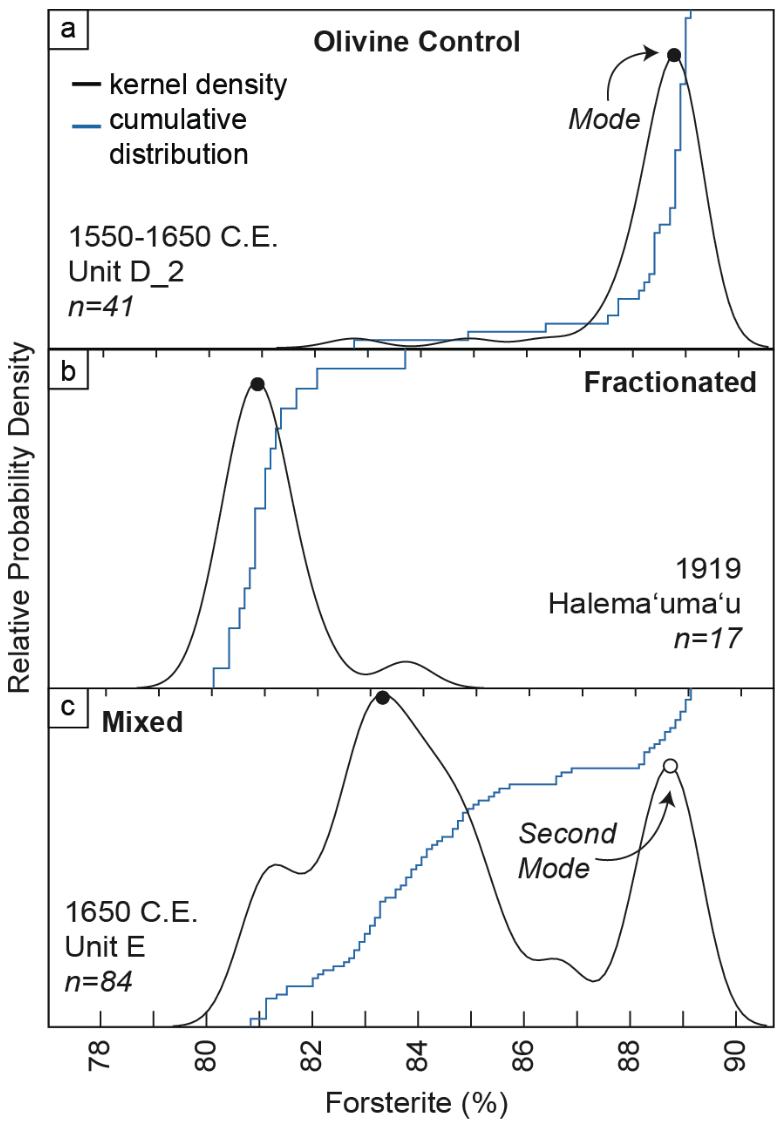

Figure 2. Examples of olivine population types used to infer magmatic processes and derive Fo modes presented in Figures 3 and 4. **(a)** Olivine-controlled eruptions like the Keanakāko'i Tephra Unit D (Lynn et al. 2017a, 2017b) typically have unimodal high-Fo populations but can exhibit a range of compositions that are present in low abundances. The mode, marked by a filled circle, is used in Figure 4 to examine long term changes in population characteristics. **(b)** Fractionated populations, like that found in the 1919 lava flow from Halemaʻumaʻu, have unimodal distributions dominated by low Fo with few higher Fo compositions. **(c)** Eruptions that reflect mixing of olivine-controlled and fractionated magmas, such as the Keanakāko'i Tephra Unit E (Lynn et al., 2017a, 2017b), have two modes with both high-Fo and low-Fo compositions

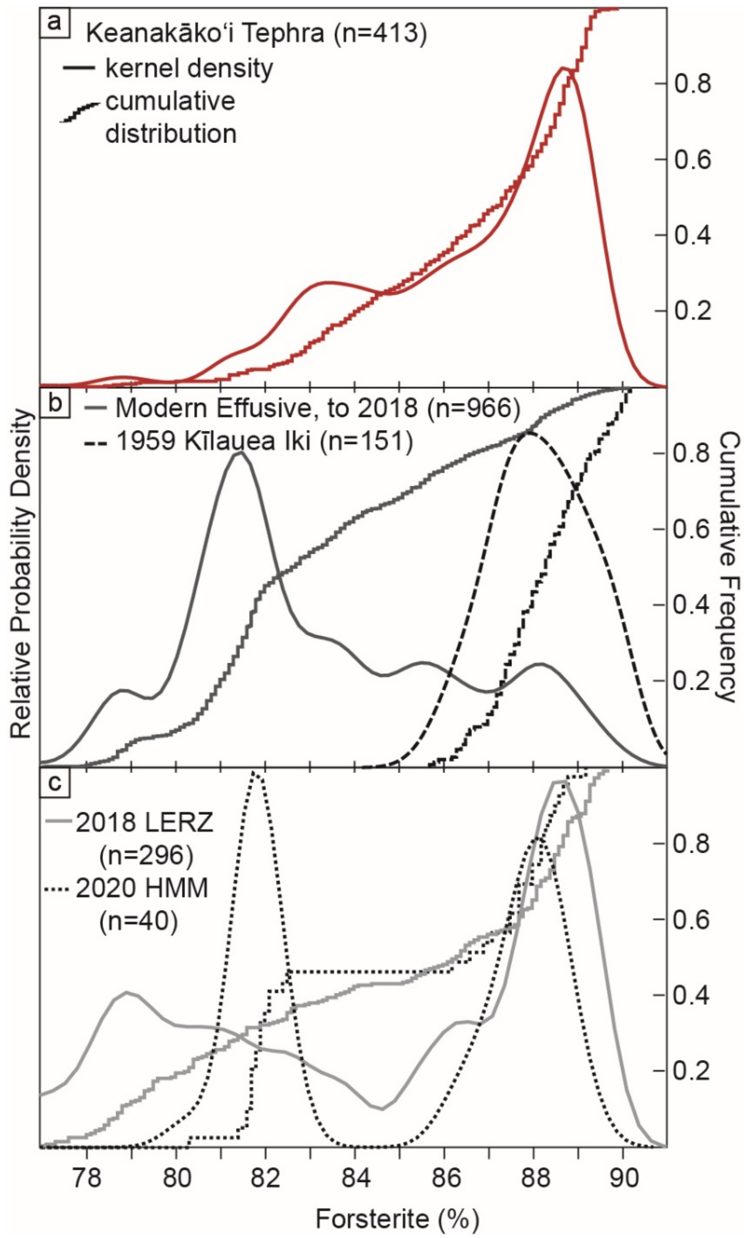

Figure 3. Olivine core compositions from ~1500 C.E. – 2020, shown as relative kernel densities and cumulative distribution functions. Data are divided into **(a)** the explosive Keanakāko'i Tephra period from ~1500 - early 1800s C.E., **(b)** the modern effusive period from ~1820s to present, excluding **(c)** the recent 2018 lower East Rift Zone (LERZ) and 2020 Halema'uma'u (HMM) eruptions.

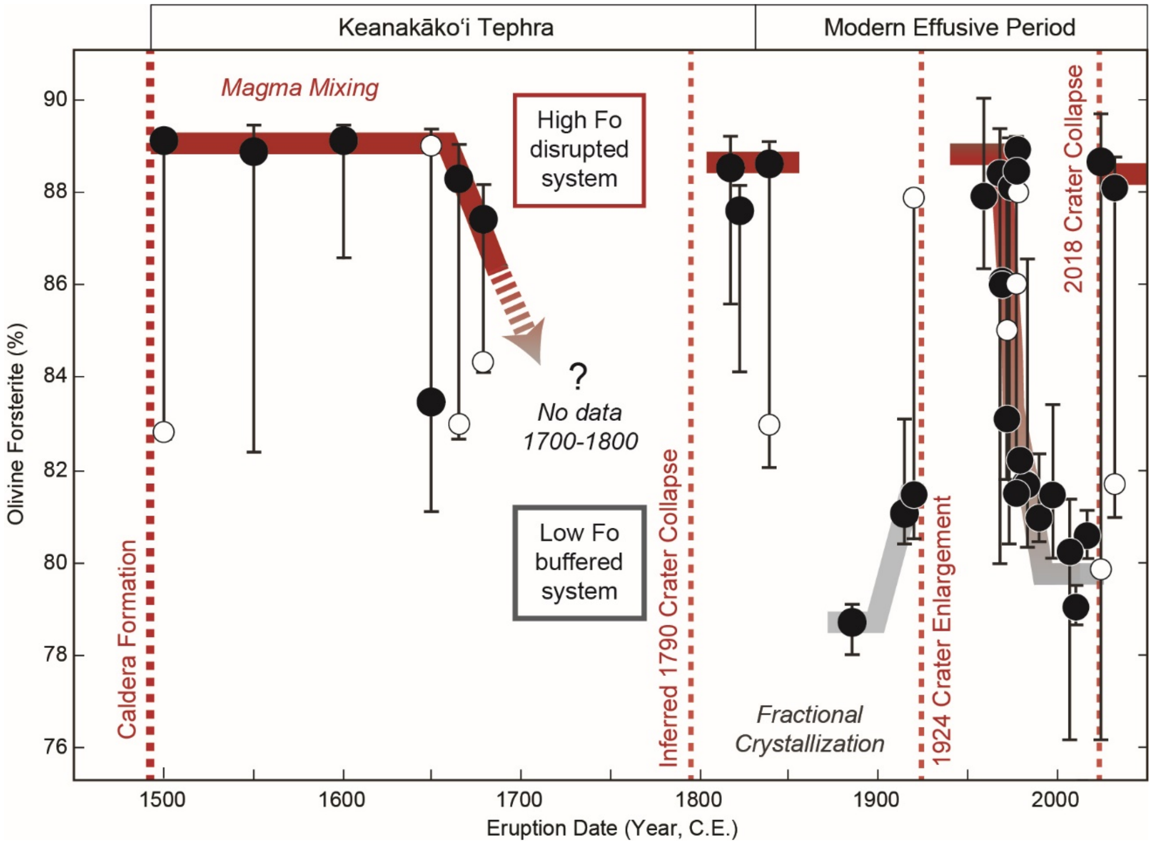

Figure 4. Olivine forsterite content variations through time. Thick dashed lines mark known or interpreted collapse events that are inferred to have disrupted the summit reservoir system. Sustained eruptions are divided into smaller time periods (e.g., Maunaulu, Puʻuʻōʻō). Data points reflect highest probability density values (see Figure 2) of olivine populations (n=17-433; see Supplementary Figures S1 and S2 for all kernel density plots and Table S3 for summary). Range bars show population data at 5th and 95th percentiles (Table S3). Data are from the following sources: 1500 - early1800s C.E. Keanakākoʻi Tephra (Lynn et al., 2017a, 2017b), 1840 upper ERZ (Trusdell, 1991), 1885 Halemaʻumaʻu (Garcia et al. 2003; this study), 1919 (Garcia et al. 2003), 1921 (Garcia et al., 2003; this study), 1959 Kīlauea Iki (Vinet and Higgins, 2011), 1969-1974 Maunaulu (Vinet and Higgins, 2010), July 1974 (Wieser et al., 2020; this study), December 1974 (Vinet and Higgins, 2010; Wieser et al., 2020), ERZ 1983-2018 (Thornber et al., 2015; Lynn et al. 2017a; Gansecki et al., 2019; Wieser et al., 2021; Lerner et al., 2021), Halemaʻumaʻu 2015-2018 (Gansecki et al., 2019; this study), and Halemaʻumaʻu 2020 (this study).

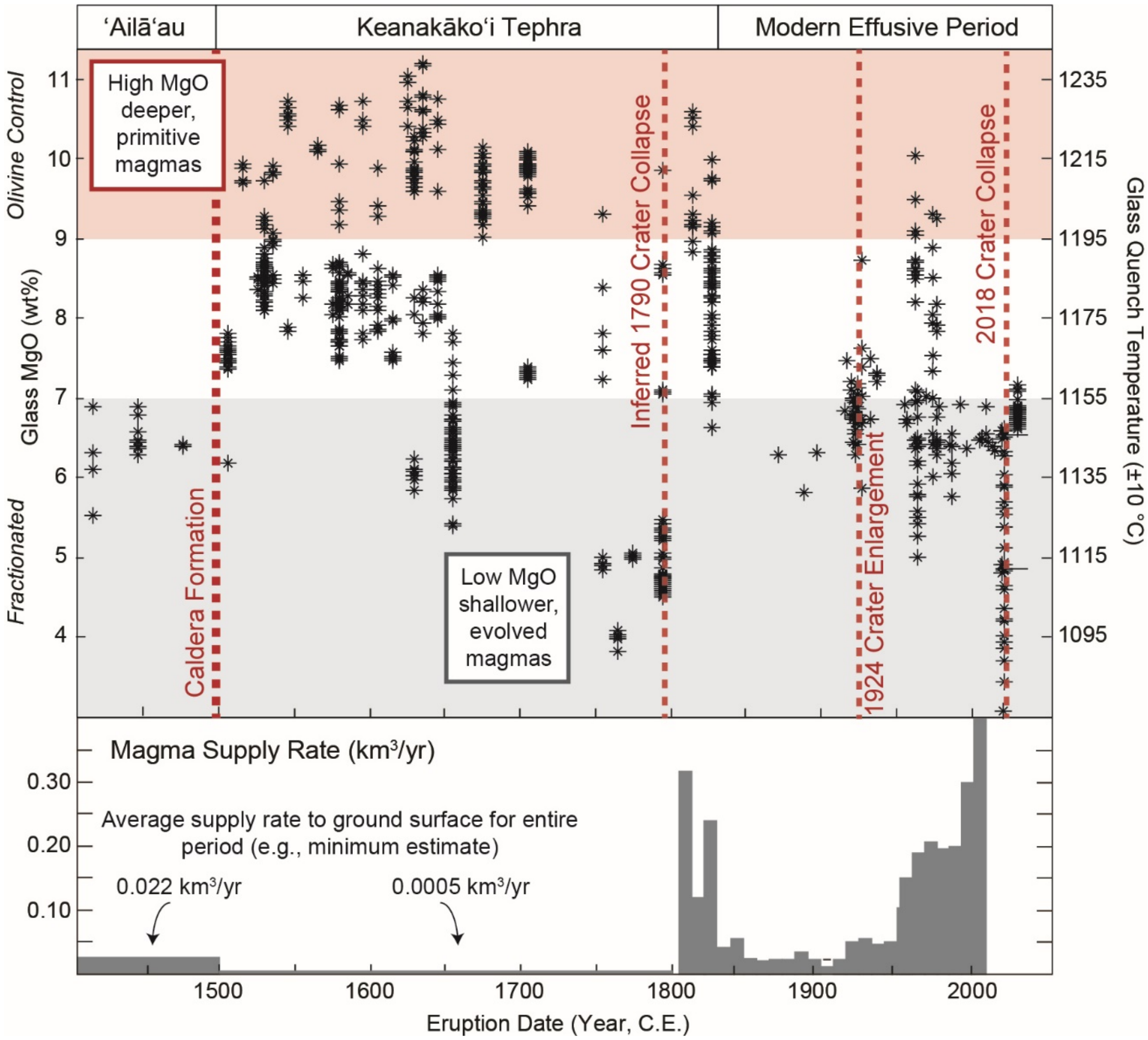

Figure 5. Glass MgO (wt%) and magma supply rate variations through time. Each glass composition is a single analysis (unlike olivine modes, above). High-MgO glasses reflect olivine control (red region; see also Figure 2) whereas low-MgO glasses are evolved due to fractional crystallization (grey region). Inferred magma supply rates for 1400-1823 are based on the volume of erupted material (Swanson et al., 2014) and calculated magma supply rates for 1823-2008 are from Wright and Klein (2014). Rates for 2003-2008 are estimated by Poland et al. (2012), and Wright and Klein (2014) noted that the use of summit CO_2 may overestimate these values. Glass data are from the following sources: ‘Ailā‘au 1410-1470 C.E. (Clague et al., 1999), 1500 – early 1800s C.E. Keanakāko‘i Tephra (Helz et al., 2014a, 2014b; Lynn et al., 2017b, Garcia et al., 2018), 1868-1982 summit (Helz, 1987; Helz et al., 1995, 2014a, 2014b; Wright and Helz, 1996; Garcia et al., 2003; Wieser et al., 2020), ERZ 1983-2018 (Helz et al., 1995; Thornber et al., 2015; Lynn et al., 2017a; Gansecki et al., 2019), and 2020 Halema‘uma‘u (this study).

Supplemental Material for:

Olivine and glass chemistry record cycles of plumbing system recovery after summit collapse events at Kīlauea Volcano, Hawai‘i

Kendra J. Lynn*, Donald A. Swanson

U.S. Geological Survey
Hawaiian Volcano Observatory
1266 Kamehameha Avenue, Suite A-8
Hilo, HI 96720

*corresponding author: klynn@usgs.gov
Keywords: olivine, caldera collapse, Kīlauea, eruptive cycles, Hawai‘i

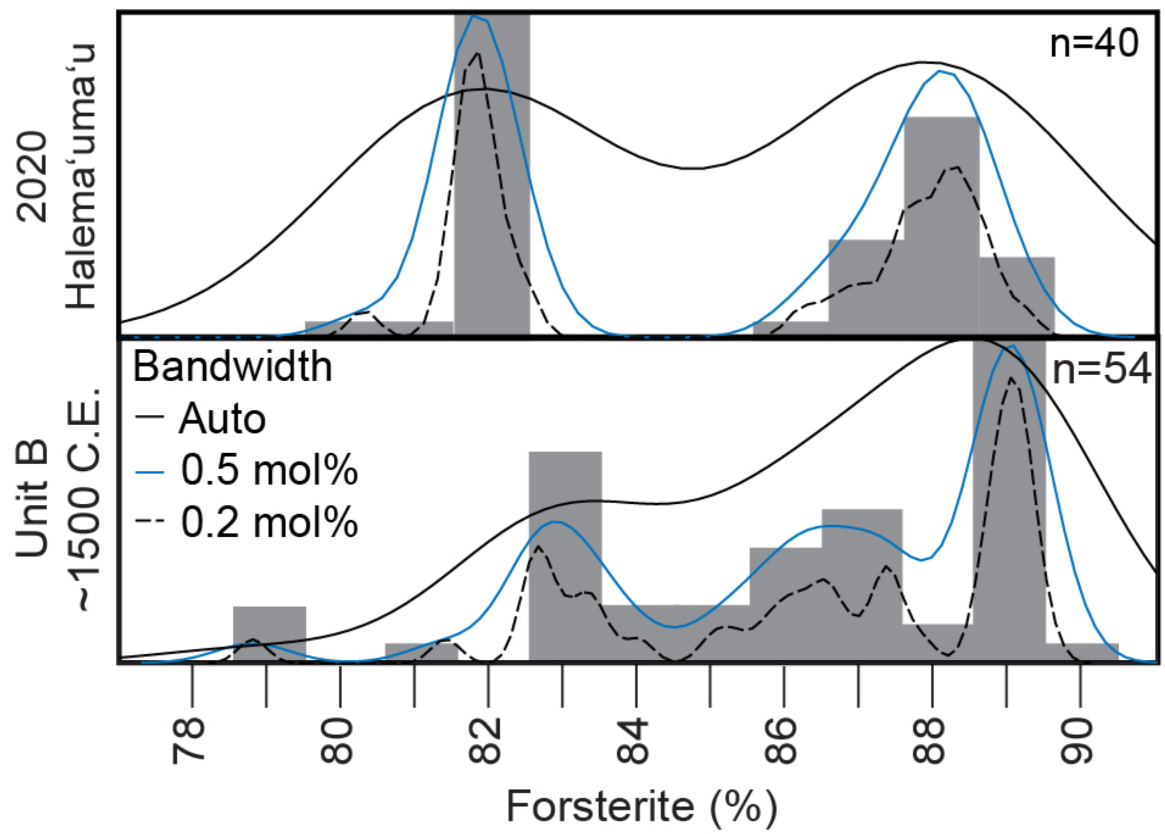

Figure S1: Comparison of kernel density estimates using different bandwidths. The bandwidth automatically selected by MATLAB (solid black line; Any use of trade, firm, or product names is for descriptive purposes only and does not imply endorsement by the U.S. Government) oversmooths the data, whereas the 0.2 mol% bandwidth (dashed black line; akin to typical analytical error) undersmooths the data. Thus, we use the 0.5 mol% bandwidth (blue line) throughout the study.

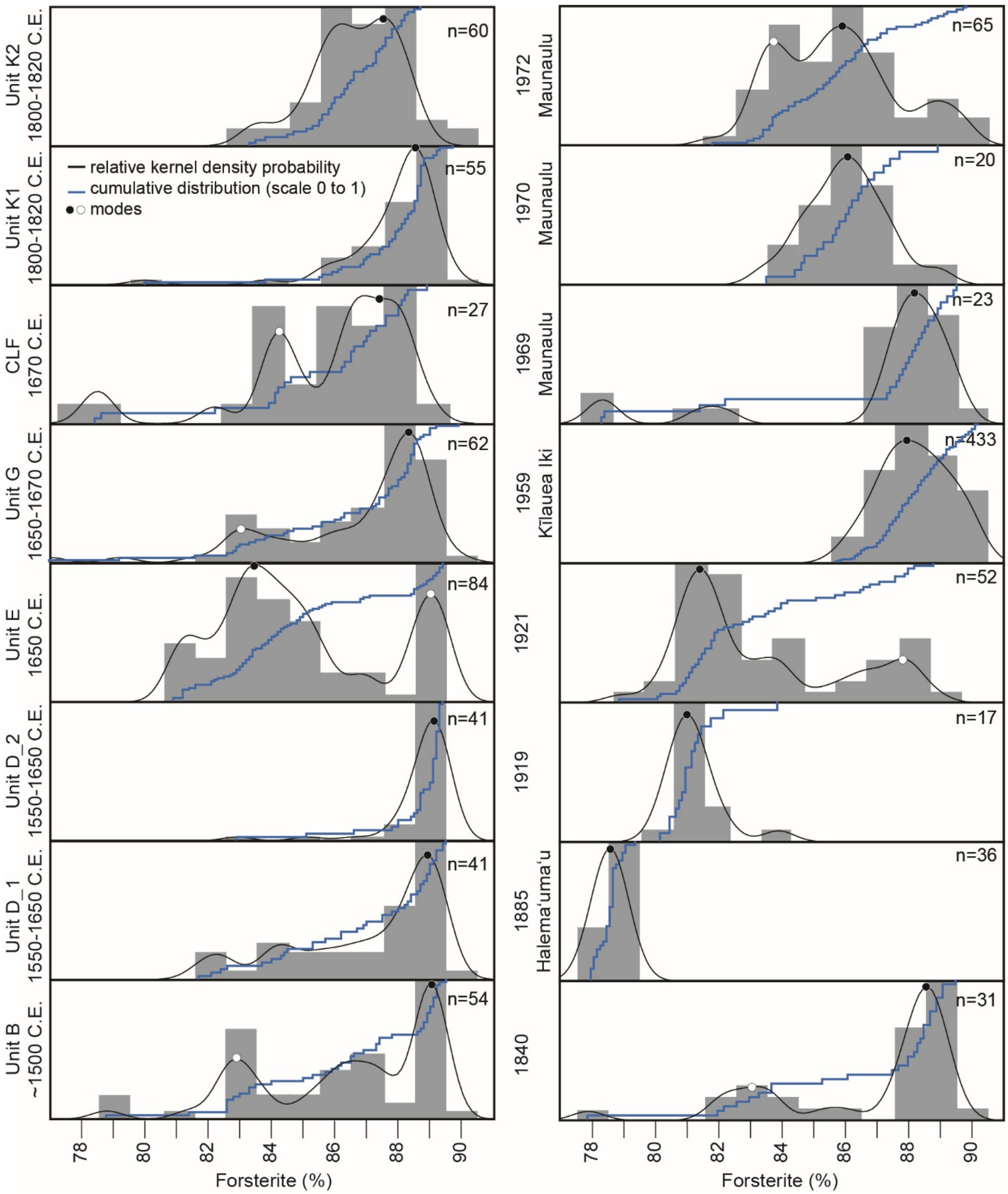

Figure S2. Olivine core Fo histograms, kernel density plots and cumulative distribution functions for each eruption in Figure 4, 1500-1972. Data are from the following sources: 1500-early 1800s C.E. Keanakākoʻi Tephra (Lynn et al., 2017b), 1840 upper ERZ (Trusdell, 1991), 1885 Halemaʻumaʻu (Garcia et al., 2003; this study), 1919 (Garcia et al., 2003), 1921 (Garcia et al., 2003; this study), 1959 Kīlauea Iki (Vinet and Higgins, 2011), 1969-1972 Maunaulu (Vinet and Higgens, 2010).

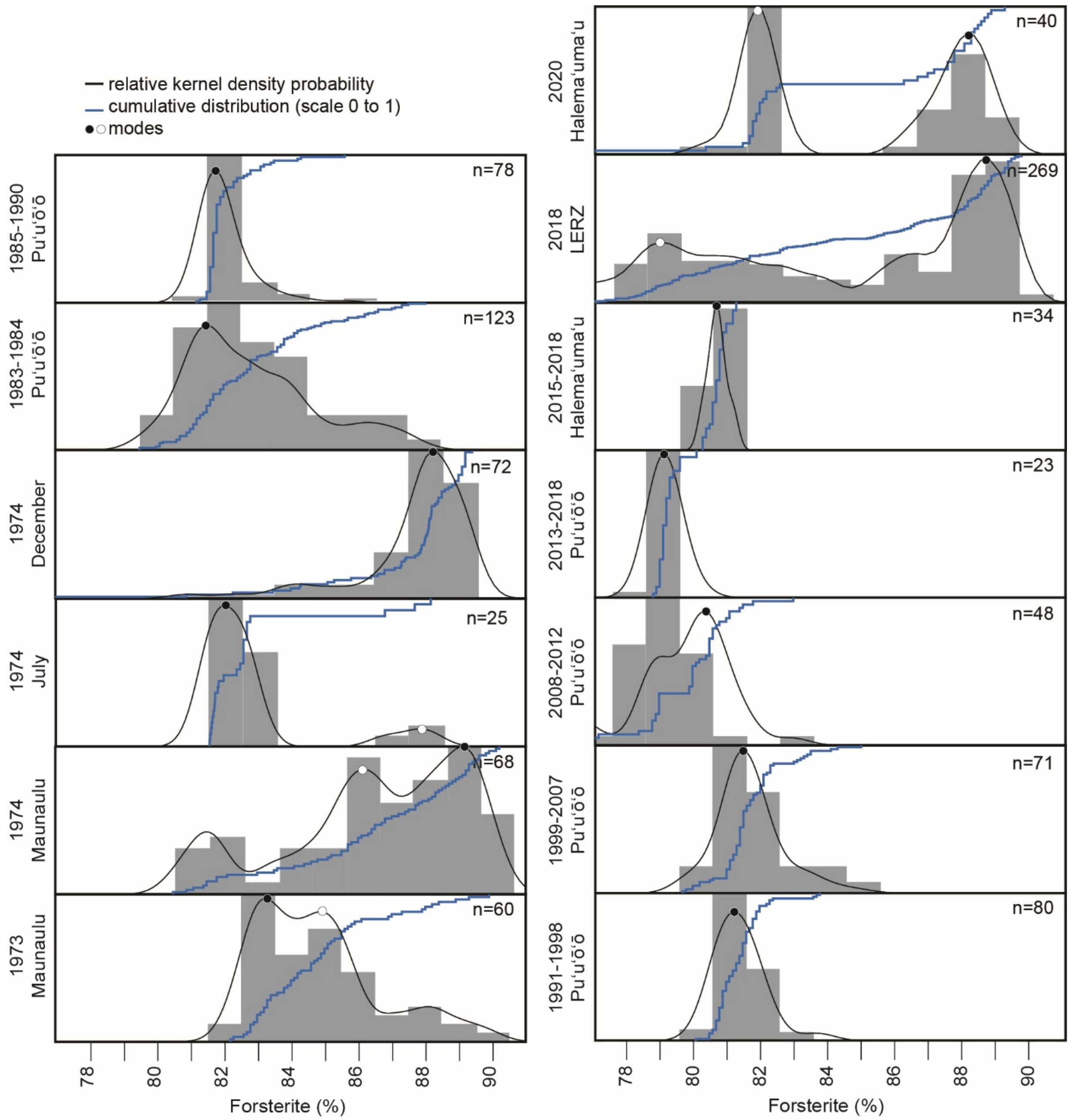

Figure S3. Olivine core Fo histograms, kernel density plots and cumulative distribution functions for each eruption in Figure 4, 1973-2020. Data are from the following sources: 1973-1974 Maunaulu (Vinet and Higgens, 2010), July 1974 (Wieser et al., 2020; this study), December 1974 (Vinet and Higgens, 2010; Wieser et al., 2020), ERZ 1983-2018 (Thornber et al., 2015; Lynn et al., 2017a; Wieser et al., 2021; Lerner et al., 2021; Gansecki et al., 2019), Halemaʻumaʻu 2015-2018 (Gansecki et al., 2019, this study), and Halemaʻumaʻu 2020 (this study).

References

Gansecki, C., Lee, R. L., Shea, T., Lundblad, S. P., Hon, K., Parcheta, C., 2019. The tangled tale of Kīlauea's 2018 eruption as told by geochemical monitoring. Science, 366, 1–9. doi: 10.1126/science.aaz0147

Garcia, M.O., Pietruszka, A.J., Rhodes, J.M., 2003. A petrologic perspective of Kīlauea Volcano's summit magma reservoir. J. Petrol. 44, 2313-2339.

Lerner, A.H., Wallace, P.J., Shea, T., Mourey, A.J., Kelly, P.J., Nadeau, P.A., Elias, T., Kern, C., Clor, L.E., Gansecki, C., Lee, R.L., Moore, L.R., Werner, C.A., 2021. The petrologic and degassing behavior of sulfur and other magmatic volatiles from the 2018 eruption of Kīlauea, Hawai‘i: melt concentrations, magma storage depths, and magma recycling. Bull. Volcanol., 83, 43. doi: 10.1007/s00445-021-01459-y

Lynn, K.J., Shea, T., Garcia, M.O., 2017a. Nickel variability in Hawaiian olivine: Evaluating the relative contributions from mantle and crustal processes. Am. Mineral., 102, 507–518. doi: 10.2138/am-2017-5763

Lynn, K.J., Garcia, M.O., Shea, T., Costa, F., Swanson, D.A., 2017b. Timescales of mixing and storage for Keanakāko‘i Tephra magmas (1500–1820 C.E.), Kīlauea Volcano, Hawai‘i. Cont. Mineral. Petrol., 172, 76. doi: 10.1007/s00410-017-1395-4

Thornber, C.R., Orr, T.R., Heliker, C., Hoblitt, R.P., 2015. Petrologic testament to changes in shallow magma storage and transport during 30+ years of recharge and eruption at Kīlauea Volcano, Hawai‘i, in Carey, R., Cayol, V., Poland, M., Weis, D., (Eds.), Hawaiian Volcanoes: From Source to Surface. AGU Geophys. Mono. 208. 147-188. doi: 10.1002/9781118872079.ch8

Trusdell, F.A., 1991, The 1840 eruption of Kilauea Volcano: Petrologic and volcanologic constraints on rift zone processes. [M.S. thesis]: Honolulu, University of Hawai‘i, 109 p.

Vinet, N., Higgins, M.D., 2010. Magma solidification processes beneath Kilauea Volcano, Hawaii: A quantitative texture and geochemical study of the 1969-1974 Mauna Ulu lavas. J. Petrol. 51, 1297-1332. doi: 10.1093/petrology/egq020

Vinet, N., Higgins, M.D., 2011. What can crystal size distributions and olivine compositions tell us about magma solidification processes inside Kilauea Iki lava lake, Hawaii? J. Volcanol. Geotherm. Res. 208, 136-162. doi: 10.1016/j.volgeores.2011.09.006

Wieser, P. E., Lamadrid, H., Maclennan, J., Edmonds, M., Matthews, S., Iacovino, K., Jenner, F. E., Gansecki, C., Trusdell, F., Lee, R. L., Ilyinskaya, E., 2021. Reconstructing Magma Storage Depths for the 2018 Kīlauean Eruption from Melt Inclusion CO2 Contents: The Importance of Vapor Bubbles. Geochem. Geophys. Geosys., 22, 1–30. doi: 10.1029/2020GC009364

Wieser, P. E., Edmonds, M., Maclennan, J., Wheeler, J., 2020. Microstructural constraints on magmatic mushes under Kīlauea Volcano, Hawai‘i. Nat. Comm., 11:14. doi: 10.1038/s41467-019-13635-y